Electronic Supplementary Material (ESI) for ChemComm.

Supporting Information

Triple bonds between iron and heavier group-14 elements in the $AFe(CO)_3^-$ complexes (A = Ge, Sn, Pb)

Jia-Qi Wang,# Chaoxian Chi,# Jun-Bo Lu, Luyan Meng, Mingbiao Luo, Han-Shi Hu,*

Mingfei Zhou,* and Jun Li

[a] Department of Chemistry & Key Laboratory of Organic Optoelectronics and Molecular Engineering of Ministry of Education, Tsinghua University, Beijing 100084, China, E-mail: hshu@mail.tsinghua.edu.cn.

[b] Jiangxi Key Laboratory for Mass Spectrometry and Instrumentation, School of Chemistry, Biological and Materials Sciences, East China University of Technology, Nanchang, Jiangxi Province 330013, China.

[c] Department of Chemistry, Collaborative Innovation Center of Chemistry for Energy Materials, Shanghai Key Laboratory of Molecular Catalysis and Innovative Materials, Fudan University, Shanghai 200433, China, E-mail: mfzhou@fudan.edu.cn.

[d] Department of Chemistry, Southern University of Science and Technology, Shenzhen 518055, China

[e] # Wang and Chi contributed equally to this work

Experimental and Theoretical Methods

Experimental: The infrared photodissociation spectra of the anion complexes were obtained by using a home-made collinear tandem time-of-flight mass spectrometer (TOFMS), which is described in detail previously.[1] The anion complexes were produced in a laser vaporization supersonic cluster source. The 1064 nm fundamental of a Nd:YAG laser was used to vaporize a rotating group-14 metal target. The heterodinuclear carbonyl anion complexes were produced from the laser vaporization process in expansions of helium seeded with 7% CO using a pulsed valve (General Valve, Series 9) at 0.3−0.7 MPa backing pressure. The iron carbonyl species were most likely formed in the gas tank or the stainless steel gas lines. The produced anions were skimmed after free expansion, and analysed by a Wiley−McLaren TOFMS. The anions of interest were each mass selected and decelerated into the extraction region of a second collinear TOFMS, where they were dissociated by a tunable IR laser. The fragment and parent anions were reaccelerated, and mass analysed by the second TOFMS. The tunable IR laser light is generated by a KTP/KTA/$AgGaSe_2$ optical parametric oscillator/amplifier system (OPO/OPA, Laser Vision) pumped by a Continuum Surelite EX Nd: YAG laser, producing about 1.0–2.0 mJ/pulse in the range of 1500–2200 cm^{-1}. The wavenumber of the OPO laser is calibrated using the CO absorptions. The photodissociation spectrum is obtained by monitoring the yield of the fragment ion as a function of the dissociation IR laser wavelength and normalizing to parent ion signal. Typical spectra were recorded by scanning the dissociation laser in steps of 2 cm^{-1} and averaging over 300 laser shots at each wavelength.

Theoretical and Computational Details. Quantum chemical calculations with consideration of scalar-relativistic (SR) effects were carried out to optimize the geometries, calculate the vibrational frequencies, and analyse the chemical bonding properties of the $AFe(CO)_3^-$ (N = C, Si, Ge, Sn, Pb, Fl) complexes using the program packages of ADF 2016,[2] Gaussian 09,[3] MOLPRO 2012,[4] and NBO 5.0.[5] The density functional theory (DFT) calculations were performed with ADF 2016, and the scalar relativistic effects were taken into account at the zero-order regular approximation (ZORA).[6] The Slater-type-orbital (STO) basis sets with the quality of triple-ζ plus two polarization functions (TZ2P) were used.[7] The frozen core approximation were applied to the [$1s^2$] shell of C and O, [$1s^2$-$2p^6$] shells of Si and Fe, [$1s^2$-$3d^{10}$] shells of Ge, [$1s^2$-$4d^{10}$] shells of Sn, and [$1s^2$-$5d^{10}$] shells of Pb.[8,9]

In the Gaussian 09 calculations, Weinhold's natural localized molecular orbitals (NLMO) analysis was performed by using the PBE functional with def2-TZVP basis set, (11s6p2d1f)/[5s3p2d1f] for the C and O, (14s9p3d1f)/[5s5p2d1f] for Si, (17s11p7d1f)/[6s4p4d1f] for Fe, (17s12p8d1f)/[6s5p4d1f] for Ge, (10s9p8d2f)/[6s5p3d2f] for Sn, and (10s9p8d2f)/[6s5p3d2f] for Pb. The relativistic effective core potentials (ECP) were applied for Ge, Sn, and Pb.[10] No relativistic spin-orbit coupling corrections were applied. The results are summarized in Table S3.

To reduce the computational cost, constrained geometry optimizations of the A-Fe bond of $AFe(CO)_3^-$ were performed at the *ab initio* CCSD(T) (coupled clusters with singles, doubles, and perturbative triples) level by fixing the bond lengths of Fe-C and C-O from B3LYP-optimized structures. The calculations were performed using the MOLPRO 2012.1 program with the cc-pVTZ(-PP) valence basis sets, (10s5p2d1f)/[4s3p2d1f] for C and O, (15s9p2d1f)/[5s4p2d1f] for Si, (20s16p8d2f1g)/[7s6p4d2f1g] for Fe, (10s11p9d1f)/ [5s4p3d1f] for Ge, (12s11p9d1f)/[5s4p3d1f] for Sn, and (12s11p8d1f)/[5s4p1d1f] for Pb (The spin-orbit averaged relativistic ECP pseudo-potential approximation was applied for Ge, Sn, and Pb elements.[11-14]) Single-point multi-configurational complete-active-space SCF (CASSCF) calculations were futher performed to examine the description of electronic configurations based on the B3LYP-optimized geometries using the same basis sets as in the Gaussian 09 calculations. The active space used 11 valence electrons in 12 orbitals (11_e,12_o), which includes six occupied orbitals and six unoccupied orbitals at the frontier region of the molecular orbitals.

Three-Orbital Interaction Model. Take $GeFe(CO)_3^-$ as an example, as shown in Figure S4(a), the energy of ψ_0 ($8a_1$) and 8e bonding orbitals significantly increase while that of antibonding 9e and ψ_2 ($17a_1$) orbitals markedly decline as lengthening the Ge-Fe bond distance, indicating the bonding and antibonding character in the orbitals respectively. The energies of remaining orbitals in Figure S4(a) (7e and ψ_1 ($9a_1$)) only have little influence by the changing of Ge-Fe bond distance, revealing the non-bonding nature of these orbitals.

The three-orbital interactions between Ge $2p_z$ and Fe $3d_z{}^2$ and $4p_z$ result in a bonding orbital (ψ_0), a nonbonding orbital (ψ_1), and an anti-bonding orbital (ψ_2), as shown in Figure S4(b), which can be understood with the first-order Hückel MO approximation. Since the s-type Fe $3d_z{}^2$ and $4p_z$ orbitals are orthogonal to each other while they both can form s-type bonding and anti-bonding combinations with the A *n*p orbital, a set of three MOs, namely *bonding* interaction [A(*n*p)+Fe(3*d*)+Fe(4*p*)], *nonbonding* [A(*n*p)-Fe(3*d*)+Fe(4*p*)], and *antibonding* [A(*n*p)-Fe(3*d*)-Fe(4*p*)], can be formed by solving the secular equation resulted from the Hückel approximation. Therefore, $8a_1$ is the s-type bonding orbital while $9a_1$ MO is largely non-bonding orbital between Fe 3*d*/4*p* and the heavier group-15 elements as has been confirmed by results shown in Figure S2 and S3. The A *np* orbital contribution in A-Fe interaction increases from C to Fl because of the increased A *np* orbital energy down the group as shown in Figure S3, which results in the gradual change of the $9a_1$ orbital from antibonding in the lighter $AFe(CO)_3^-$ complexes to nonbonding in the heavier analogues. Since each of the $8a_1$ and 8e orbitals that are A-Fe bonding in character are doubly occupied, the A-Fe bonds can thus be regarded as triple bonds involving one σ bond and two π bonds. The triple bond assignment is also verified by the natural localized MO (NLMO) analysis (Table S4), which reveals a weakly polarized, covalent A-Fe σ orbital composed of about 40% Fe and 56% A character and two strongly polarized, inverse-dative π bonds composed of about 80% Fe and 12% A character. Population analysis indicates that the unpaired spin is largely located on the $Fe(CO)_3^-$ fragment. Accordingly, the ground state $AFe(CO)_3^-$ anion complexes can be regarded as being resulted from the interactions between the A atoms in the ^3P ground state with $(np)^2$ configuration and the $Fe(CO)_3^-$ fragment in an ^4E excited spin state in $(7e)^4(8e)^3$ $(7a_1)^1(8a_1)^1$ configuration in forming one σ and two π bonds.

References

[1] G. J. Wang, C. X. Chi, X. P. Xing, C. F. Ding, M. F. Zhou, *Sci. China Chem.* **2014**, *57*, 172–177.

[2] ADF 2016.101, http://www.scm.com.

[3] M. Frisch, G. Trucks, H. B. Schlegel, G. E. Scuseria, M. A. Robb, J. R. Cheeseman, G. Scalmani, V. Barone, B. Mennucci, G. Petersson, Gaussian, Inc., Wallingford CT, **2009**.

[4] H. J. Werner, *et al*. MOLPRO, version 2008.1, Univ. College Cardiff Consultants Limited, Cardiff, U.K., http://www.molpro.net.

[5] Glendening, E. D.; et al. NBO 5.0; Theoretical Chemistry Institute, University of Wisconsin: Madison, WI, 2004.

[6] E. van Lenthe, E. J. Baerends, J. G. Snijders, *J. Chem. Phys.* **1993**, *99*, 4597-4610.

[7] E. van Lenthe, E. J. Baerends, *J. Comput. Chem.* **2003***, 24*, 1142-1156.

[8] A. E. Reed, F. Weinhold, *J. Chem. Phys.* **1985**, *83*, 1736-1740.

[9] K. A. Peterson, D. Figgen, E. Goll, H. Stoll, M. Dolg, *J. Chem. Phys.* **2003**, *119*, 11113-11123.

[10] a) A. Schaefer, C. Huber, R. Ahlrichs, *J. Chem. Phys.* **1994**, *100,* 5829-5835; b) F. Weigend, R. Ahlrichs, *Phys. Chem. Chem. Phys.* **2005**, *7,* 3297-3305.

[11] T. H. Dunning, *J. Chem. Phys.* **1989**, *90*, 1007-1023.

[12] D. E. Woon, T. H. Dunning, *J. Chem. Phys.* **1993**, *98*, 1358-1371.

[13] N. B. Balabanov, K. A. Peterson, *J. Chem. Phys.* **2005**, *123*, 064107.

[14] K. A. Peterson, *J. Chem. Phys.* **2003**, *119*, 11099-11112.

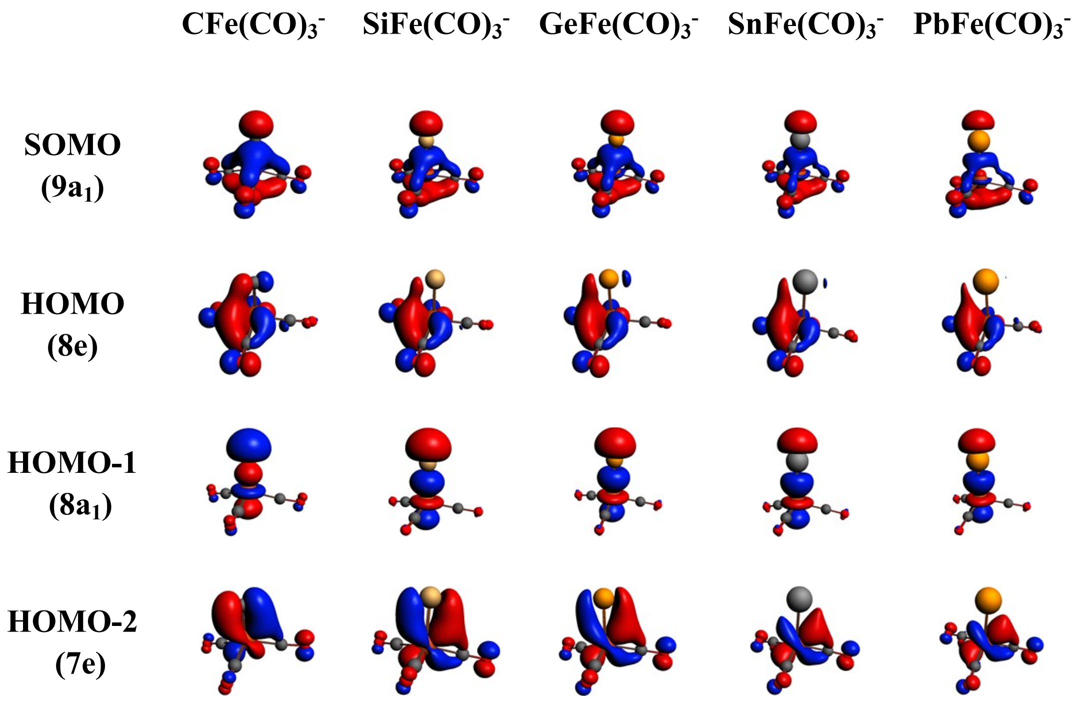

Figure S1. Upper occupied canonical Kohn-Sham valence MO orbitals of $AFe(CO)_3^-$ (A = C, Si, Ge, Sn, and Pb; Isosurfaces = 0.05 au). For the degenerate 7e δ-type and 8e π-type MOs, only one set is shown.

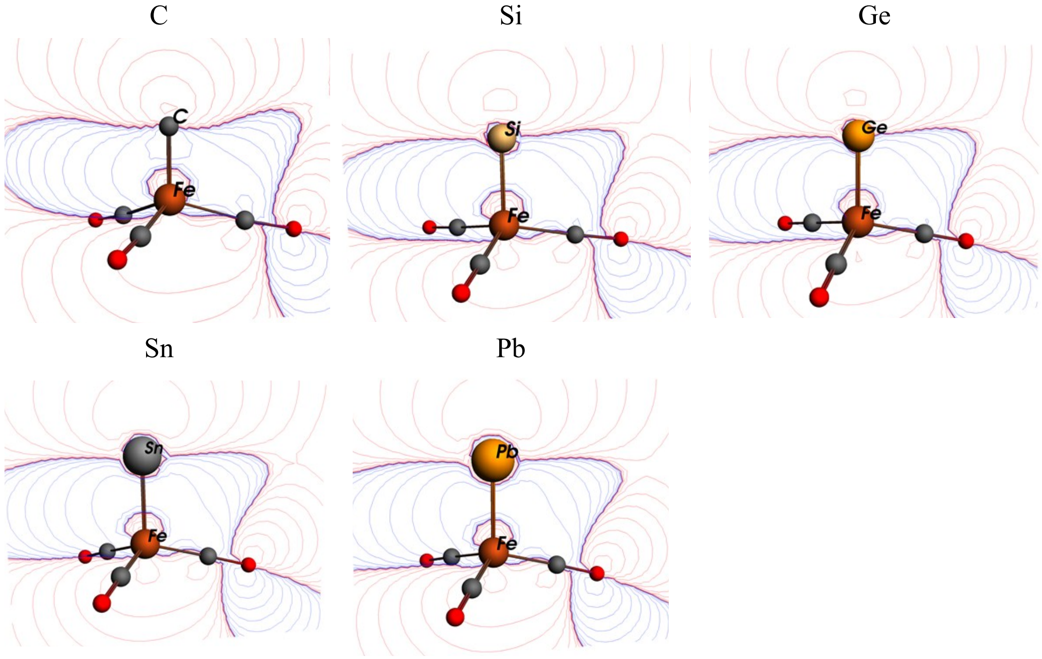

Figure S2. The 2D-contours of $9a_1$ orbitals of $AFe(CO)_3^-$ (A = C, Si, Ge, Sn, Pb) (cutoff = 0.05 au).

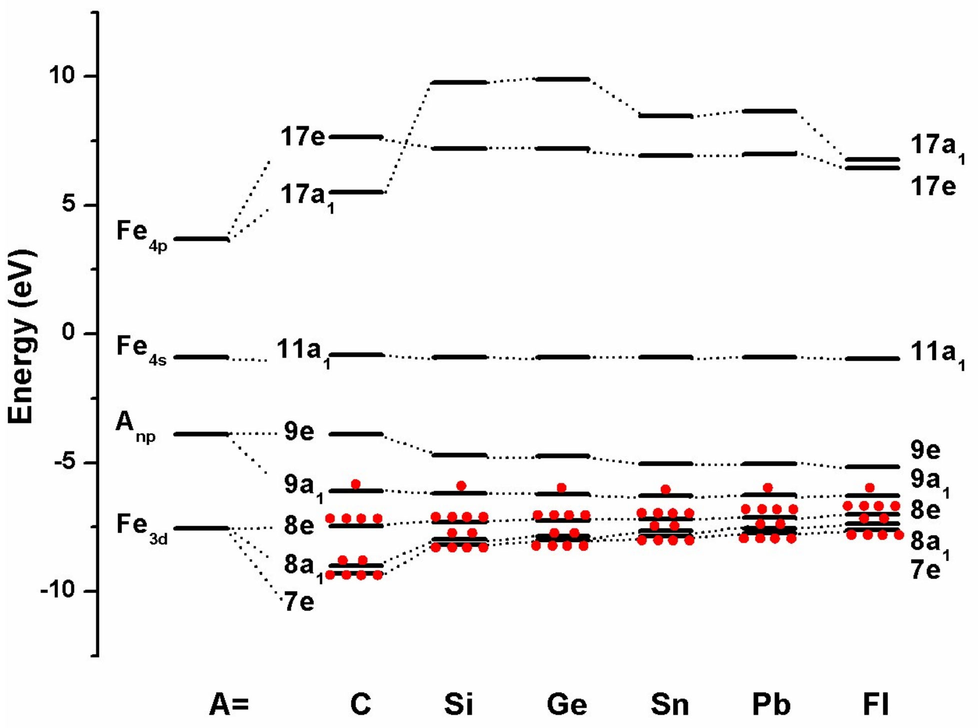

Figure S3. The scalar-relativistic PBE/TZ2P energy levels of AFe(CO)$_3^-$ (A = C, Si, Ge, Sn, Pb, Fl). The 9a$_1$ orbital is stabilized from C to Fl.

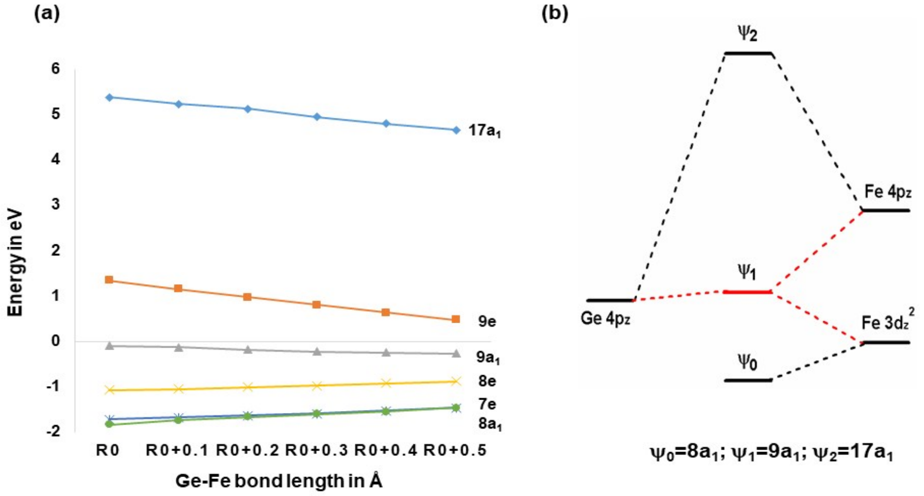

Figure S4. (a) The frontier MO energy levels (PBE/TZ2P) of $GeFe(CO)_3^-$ as lengthening Ge-Fe bond distance by 0.1 Å in each step. (b) The σ-type three-orbital interaction among Ge $4p_z$ and Fe $3d_z{}^2$ and $4p_z$ of $Fe(CO)_3^-$.

Table S1. Calculated relative binding energies (kcal.mol^{-1}) for different spin multiplicities of AFe(CO)$_3^-$ (A = C, Si, Ge, Sn, Pb) at the DFT SR-ZORA PBE/TZ2P level of theory.

Molecular symmetry	State	Structure	ΔE
CFe(CO)$_3^-$ (C_{3v})	$^2A_1$	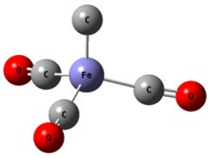	0
	^4E		68.27
	$^6A_1$		88.63
SiFe(CO)$_3^-$ (C_{3v})	$^2A_1$	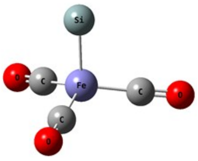	0
	^4E		44.66
	$^6A_1$		61.43
GeFe(CO)$_3^-$ (C_{3v})	$^2A_1$	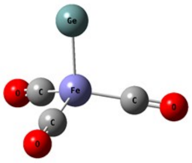	0
	^4E		43.62
	$^6A_1$		57.36
SnFe(CO)$_3^-$ (C_{3v})	$^2A_1$	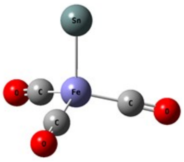	0
	^4E		35.40
	$^6A_1$		46.31
PbFe(CO)$_3^-$ (C_{3v})	$^2A_1$	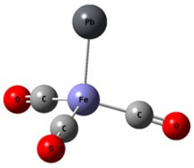	0
	^4E		33.39
	$^6A_1$		43.81

Table S2. Natural valence orbitals of the $AFe(CO)_3^-$ (A = C, Si, Ge, Sn, Pb) from CASSCF (11_e,12_o): natural orbital occupation numbers (NOON) and contour surfaces (0.05 au).*

	NOON				
NO	C	Si	Ge	Sn	Pb
12	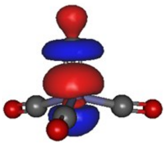 0.0052	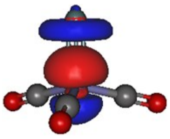 0.0055	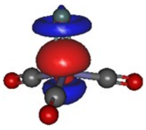 0.0057	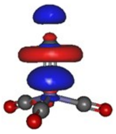 0.0059	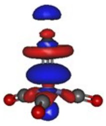 0.0054
11	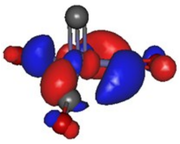 0.0783	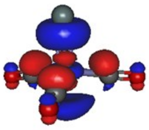 0.0745	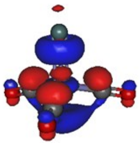 0.0724	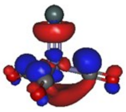 0.0168	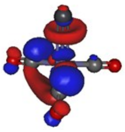 0.0168
10	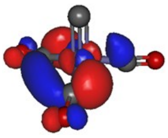 0.0783	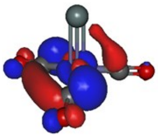 0.0840	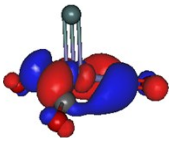 0.0809	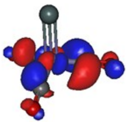 0.0884	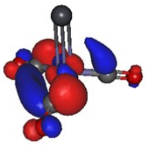 0.0919
9	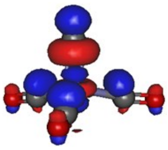 0.0821	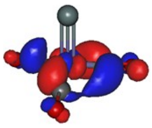 0.0845	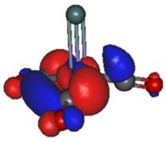 0.0809	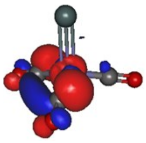 0.0962	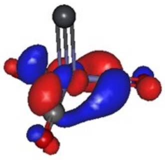 0.0988
8	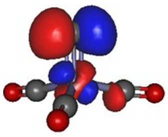 0.1107	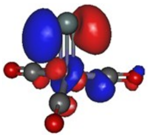 0.1142	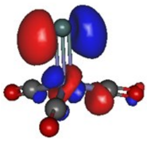 0.1084	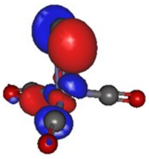 0.1315	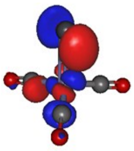 0.1325
7	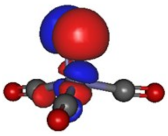 0.1107	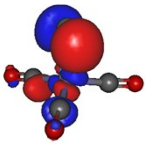 0.1142	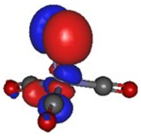 0.1084	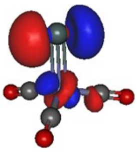 0.1608	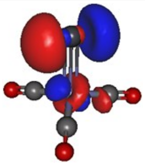 0.1696
6	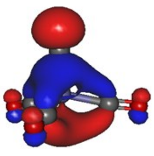 1.0079	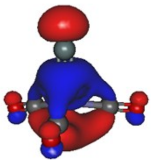 1.0218	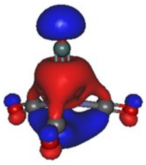 1.0137	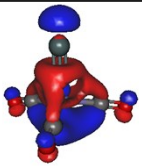 1.0300	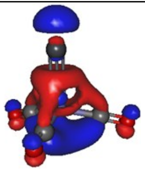 1.0326

5	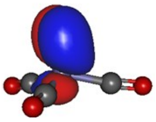 1.8906	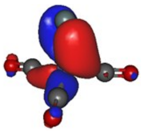 1.8698	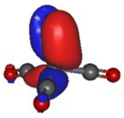 1.8925	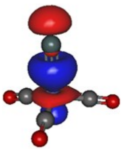 1.8282	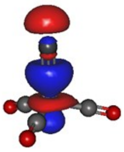 1.8181
4	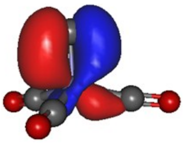 1.8906	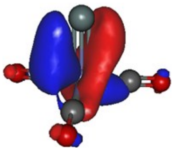 1.8875	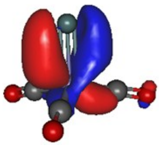 1.8925	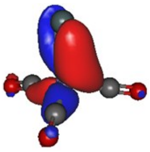 1.8731	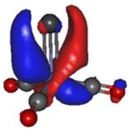 1.8650
3	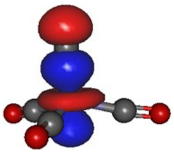 1.9104	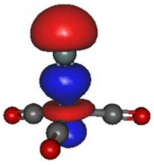 1.8933	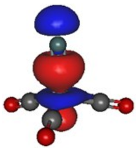 1.9123	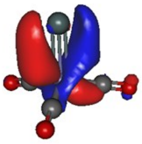 1.8766	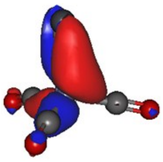 1.8704
2	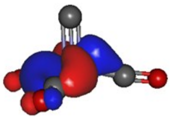 1.9213	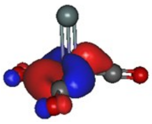 1.9152	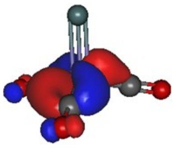 1.9186	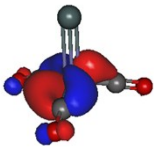 1.9059	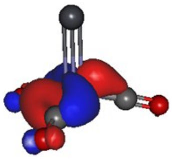 1.9064
1	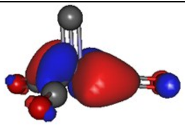 1.9213	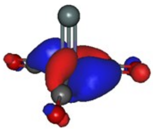 1.9155	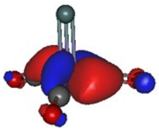 1.9187	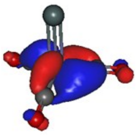 1.9062	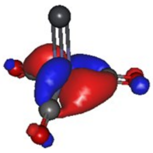 1.9068
C_0^2	0.81	0.81	0.81	0.77	0.76
EBO	2.7	2.7	2.7	2.6	2.6

* C_0^2 is the weight of the leading configuration. EBO is the effective bond order from CASSCF calculations.

Table S3. AO contributions (in %) in KS-MOs of AFe(CO)$_3^-$ (A = C, Si, Ge, Sn, Pb) at the PBE/TZ2P level of theory.

$^2A_1$ C_{3v}-CFe(CO)$_3^-$						
	C		Fe			CO
	2p	2s	4s	3d	4p	
SOMO 9a$_1$	30.7		1.7	5.6	11.9	50.1
HOMO 8e	8.7			48.8	10.3	40.9
HOMO-1 8a$_1$	34.3			41.7	1.1	22.9
HOMO-2 7e	26.4			60.5	3.0	10.1
HOMO-3 6e				20.4	4.9	74.7
$^2A_1$ C_{3v}-SiFe(CO)$_3^-$						
	Si		Fe			CO
	3p	3s	4s	3d	4p	
SOMO 9a$_1$	30.5			7.6	15.5	46.4
HOMO 8e	9.9			45.7	11.1	33.3
HOMO-1 8a$_1$	32.6	7.3	1.7	53.1		5.3
HOMO-2 7e	16.1			65.9	2.5	15.5
HOMO-3 6e				17.8	5.7	76.5
$^2A_1$ C_{3v}-GeFe(CO)$_3^-$						
	Ge		Fe			CO
	4p	4s	4s	3d	4p	
SOMO 9a$_1$	33.1			7.0	15.9	
HOMO 8e	13.6			44.4	12.0	30.0
HOMO-1 8a$_1$	33.9	3.8		55.6		10.5
HOMO-2 7e	14.0			67.8	1.2	17.0
HOMO-3 6e				18.2	5.4	76.4
$^2A_1$ C_{3v}-SnFe(CO)$_3^-$						
	Sn		Fe			CO
	5p	4s	4s	3d	4p	
SOMO 9a$_1$	34.7			7.4	16.9	41.0
HOMO 8e	17.3			39.9	12.6	30.2
HOMO-1 8a$_1$	32.4	3.3	1.2	57.6		5.5
HOMO-2 7e	10.2			70.1		19.7
HOMO-3 6e				18.2	5.4	76.4
$^2A_1$ C_{3v}-PbFe(CO)$_3^-$						
	Pb		Fe			CO
	6p	6s	4s	3d	4p	
SOMO 9a$_1$	34.2			7.2	17.0	41.6
HOMO 8e	18.5			39.0	12.4	30.1
HOMO-1 8a$_1$	32.7	2.0	1.2	59.4		4.7
HOMO-2 7e	8.7			70.9		20.4
HOMO-3 6e				18.0	5.3	76.7

Table S4. The calculated natural localized molecular orbitals (NLMOs) of $AFe(CO)_3^-$ (A=C, Si, Ge, Sn, Pb) using def2-TZVP basis sets.

Orbital	$CFe(CO)_3^-$	$SiFe(CO)_3^-$	$GeFe(CO)_3^-$	$SnFe(CO)_3^-$	$PbFe(CO)_3^-$
A-Fe σ	50.2%Fe($s^{0.08}d^{1.00}$)+ 47.7%C($s^{0.29}p^{1.00}$)	39.4%Fe($s^{0.16}d^{1.00}$)+ 58.5%Si($s^{0.36}p^{1.00}$)	39.4%Fe($s^{0.16}d^{1.00}$)+ 58.5%Ge($s^{0.36}p^{1.00}$)	41.9%Fe($s^{0.19}d^{1.00}$)+ 56.0%Sn($s^{0.17}p^{1.00}$)	42.5%Fe($s^{0.13}d^{1.00}$)+ 55.5%Pb($s^{0.18}p^{1.00}$)
A-Fe π	76.2%Fe($d^{1.00}$)+ 18.2%C($p^{1.00}$)	79.4%Fe($d^{1.00}$) + 11.3%Si($p^{1.00}$)	79.4%Fe($d^{1.00}$) + 11.3%Ge($p^{1.00}$)	77.7%Fe($d^{1.00}$) + 12.4%Sn($p^{1.00}$)	77.1%Fe($d^{1.00}$) + 12.8%Pb($p^{1.00}$)
A-C σ	29.0%Fe($d^{1.00}$)+ 16.2%C′ ($s^{0.25}p^{1.00}$)+ 12.7%C($p^{1.00}$)	27.1%Fe($d^{1.00}$)+ 21.9%Si($s^{0.20}p^{1.00}$)+ 12.3%C($p^{1.00}$)	29.3%Fe($d^{1.00}$)+ 21.4%Ge($s^{0.15}p^{1.00}$)+ 11.7%C($p^{1.00}$)	32.2%Fe($d^{1.00}$)+ 21.3%Sn($s^{0.14}p^{1.00}$)+ 10.9%C($p^{1.00}$)	28.9%Fe($d^{1.00}$)+ 23.5%Pb($s^{0.18}p^{1.00}$)+ 13.0%C($s^{0.13}p^{1.00}$)

Table S5. Energy decomposition analysis of $AFe(CO)_3^-$ at the DFT PBE/TZ2P level. Energy values are given in kcal mol^{-1}.

Interaction fragments	$CFe(CO)_3^-$ C (^3P) + $Fe(CO)_3^-$ (^4E)	$SiFe(CO)_3^-$ Si ((^3P) + $Fe(CO)_3^-$ (^4E)	$GeFe(CO)_3^-$ Ge ((^3P) + $Fe(CO)_3^-$ (^4E)	$SnFe(CO)_3^-$ Sn ((^3P) + $Fe(CO)_3^-$ (^4E)	$PbFe(CO)_3^-$ Pb ((^3P) + $Fe(CO)_3^-$ (^4E)
ΔE_{int}	-175.9	-126.0	-120.0	-103.8	-98.6
$\Delta E_{\mathrm{Pauli}}$	372.7	268.0	253.9	232.8	228.8
$\Delta E_{\mathrm{elstat}}{}^{a}$	-241.3 (44.0%)	-211.4 (53.7%)	-207.4 (55.5%)	-198.5 (59.0%)	-198.2 (60.5%)
$\Delta E_{\mathrm{orb}}{}^{a}$	-307.2 (56.0%)	-182.6 (46.3%)	-166.5 (44.5%)	-138.0 (41.0%)	-129.3 (39.5%)
$\Delta E_{\mathrm{orb}(\sigma)}{}^{b}$	-149.8 (48.8%)	-88.0 (48.2%)	-84.1 (50.5%)	-71.4 (51.7%)	-66.7 (51.6%)
$\Delta E_{\mathrm{orb}(\pi\perp)}{}^{b}$	-58.1 (18.9%)	-45.2 (24.7%)	-38.3(23.0%)	-31.8 (23.0%)	-31.0 (24.0%)
$\Delta E_{\mathrm{orb}(\pi//)}{}^{b}$	-90.5 (29.5%)	-40.1 (22.0%)	-36.9 (22.2%)	-29.3 (22.0%)	-25.7 (19.9%)
$\Delta E_{\mathrm{orb}(\delta\perp)}{}^{b}$	-4.2 (1.4%)	-5.1 (2.8%)	-3.9 (2.4%)	-3.30 (2.4%)	-2.9 (2.2%)
$\Delta E_{\mathrm{orb}(\delta//)}{}^{b}$	-1.7 (0.6%)	-1.7 (0.9%)	-1.6 (0.9%)	-1.4 (1.0%)	-1.2 (0.9%)
ΔE_{prep}	18.3	17.3	16.9	16.1	16.8
$\Delta E_{\mathrm{tot\text{-}bonding}}{}^{c}$	-157.5	-108.7	-103.7	-87.7	-81.8

[a] The value in parentheses gives the percentage contribution to the total attractive interactions $\Delta E_{\mathrm{elstat}}+\Delta E_{\mathrm{orb}}$. [b] The value in parentheses gives the percentage contribution to the total orbital interactions ΔE_{orb}. [c] $\Delta E_{\mathrm{tot\text{-}bonding}} = \Delta E_{\mathrm{prep}} + \Delta E_{\mathrm{int}}$

Table S6. Deformation densities ($\Delta\rho$, isosurface=0.04) of the most important pairwise orbital interactions σ, $\pi_{\perp}$, $\pi_{//}$ (see Table S5) of EDA-NOCV analysis (charge density flow from red to blue).

Term	$CFe(CO)_3^-$	$SiFe(CO)_3^-$	$GeFe(CO)_3^-$	$SnFe(CO)_3^-$	$PbFe(CO)_3^-$
$\Delta E_{orb(\sigma)}{}^b$	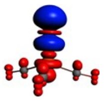 (-149.8, 48.8%)	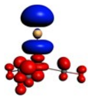 (-88.0, 48.2%)	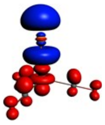 (-84.1, 50.5%)	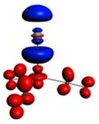 (-71.4, 51.7%)	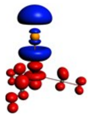 (-66.7, 51.6%)
$\Delta E_{orb(\pi\perp)}{}^b$	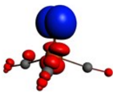 (-58.1, 18.9%)	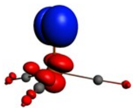 (-45.2, 24.7%)	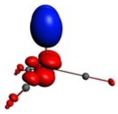 (-38.3, 23.0%)	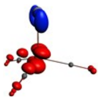 (-31.8, 23.0%)	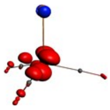 (-31.0, 24.0%)
$\Delta E_{orb(\pi//)}{}^b$	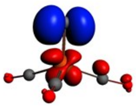 (-90.5, 29.5%)	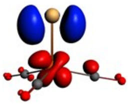 (-40.1, 22.0%)	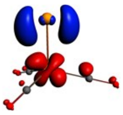 (-36.9, 22.2%)	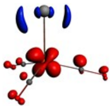 (-29.3, 22.0%)	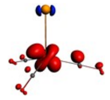 (-25.7, 19.9%)

The values in parentheses gives the corresponding eigenvalues and the percentage contributions to the total orbital interactions ΔE_{orb}.